Commun. Comput. Phys.
doi: 10.4208/cicp.011010.280611s

Vol. **12**, No. 3, pp. 789-806
September 2012

Numerical Simulation of Glottal Flow in Interaction with Self Oscillating Vocal Folds: Comparison of Finite Element Approximation with a Simplified Model

P. Sváček[1,*] and J. Horáček[2]

[1] *Department of Technical Mathematics, Faculty of Mechanical Engineering, Czech Technical University in Prague, Karlovo nám. 13, Praha 2, 121 35, Czech Republic.*
[2] *Institute of Thermomechanics, Academy of Sciences of the Czech Republic, Dolejškova 5, Praha 8, Czech Republic.*

Received 1 October 2010; Accepted (in revised version) 28 June 2011

Available online 1 March 2012

Abstract. In this paper the numerical method for solution of an aeroelastic model describing the interactions of air flow with vocal folds is described. The flow is modelled by the incompressible Navier-Stokes equations spatially discretized with the aid of the stabilized finite element method. The motion of the computational domain is treated with the aid of the Arbitrary Lagrangian Eulerian method. The structure dynamics is replaced by a mechanically equivalent system with the two degrees of freedom governed by a system of ordinary differential equations and discretized in time with the aid of an implicit multistep method and strongly coupled with the flow model. The influence of inlet/outlet boundary conditions is studied and the numerical analysis is performed and compared to the related results from literature.

AMS subject classifications: 74F10, 65Z05, 76D05

Key words: Finite element method, arbitrary Lagrangian-Eulerian method, biomechanics of voice production.

1 Introduction

The flow induced vibrations of structures can be important in various situations and technical applications, for an overview see e.g. [3]. The research focuses on problems of fluid-structure interactions (FSI) in aero-elasticity and hydro-elasticity [9]. Recently, the numerical methods for solution of FSI problems become important also in biomechanics. One approach in speech modelling is to model the interaction of the vocal folds using a

*Corresponding author. *Email addresses:* Petr.Svacek@fs.cvut.cz (P. Sváček), jaromirh@it.cas.cz (J. Horáček)

simplified model, cf. [17], based on a simplified description of both fluid and structure dynamics. Recently, simplified methods for numerical analysis of interactions of glottal flow with vocal folds vibrations were used e.g. in [14, 16]. Even if for these approaches a simplification of the flow problem was used, e.g. potential flow or Bernoulli equation, such simplified models are able to quantify many fundamental physical parameters characterizing the human voice production known in phoniatrics – see e.g. applications of the developed aeroelastic model [15] in simulations of phonation [1] and the vocal folds loading [12, 13]. The reality is much more complex: the air flow coming from lungs accelerates in the narrowest glottal part causing the vibrations of the vocal folds compliant tissue. The glottis is almost (or completely) closing during vibrations and the vocal folds collide generating the sound. The modelling of such a complex phenomenon encounters many difficulties as it is a result of coupling complex fluid dynamics and structural behaviour including contact and acoustic problems. Recently, more accurate flow descriptions were used to improve flow calculations, cf. [20]. Particularly, the interaction of air flow in human vocal tract with the vibration of the vocal folds was considered in [18].

Nevertheless, the application of simplified mathematical models can provide valuable information as well as better understanding of the phenomena. Particularly, the numerical simulations are considered as important tool in biomechanics, where experimental in-vivo studies are problematic. In this paper the coupled FSI problem of air flow through model of the vibrating glottal region is numerically approximated in a simplified geometrical domain. The results are compared to the relevant results obtained by a simplified flow model and attention is paid to the comparison of approximate solutions of the coupled fluid-structure interaction problem to the outcomes of a simplified aeroelastic model. Similar comparisons were published in [8], where the finite volume approximations of Navier-Stokes equations on Cartesian grids were coupled with a two-mass dynamical model, cf. [17]. Here, the 2D finite element approximations of Navier-Stokes equations are coupled with the elastic structure vibrations described by a mechanically equivalent two degrees of freedom system. Such a problem was analyzed in [14], [16] using a simplified 1D flow model allowing the self-sustained vibrations (i.e. the critical flow velocity for which the system becomes unstable by flutter type of instability).

The flow is described by the incompressible Navier-Stokes equations (flow velocities in the human glottal region are lower than 100 m/s and the influence of compressibility on the flow induced instability can be neglected). The flow problem is numerically approximated by the finite element (FE) method stabilized by Galerkin-Least Squares (GLS) method, cf. [6, 10], and modified for the application on moving domains, cf. [21]. Furthermore, the time and space discretized linearized problem of the large system of linear equations needs to be solved in a fast and efficient manner. The application of direct solvers as UMFPACK (cf. [7]) leads to a robust method, where different stabilization procedures can be easily applied even on anisotropically refined grids. The system of ordinary differential equations describing the structure motion is discretized in time by higher order backward difference formulas (2nd or 4th order). The fluid and structure are coupled by the interface conditions enforced by a coupling algorithm. The described

developed methodology is applied on the relevant benchmark from literature and the numerical results are presented.

2 Mathematical model

2.1 Geometry of the channel

A simplified geometry of the channel is chosen and given by the shape of the vocal folds (see Figs. 1, 2, 3). The vocal folds geometry depends on the tension of the vocal folds and varies with the fundamental vibration frequency, loudness and mode of phonation. For the purposes of numerical analysis in this paper the geometry of the vocal folds was chosen as linear function according to [15, 22] as

$$a_f(x) = 0.77120x \text{ [m]}$$

(linear shape, approximation of the vocal fold for *female* – model F) or the vocal fold with intermediate bulging approximated in [15] according to [4] as

$$a_m(x) = 1.858x - 159.861x^2 \text{ [m]}$$

(parabolic shape, approximation of the vocal fold for *male* – model M), see Figs. 1 and 2. Here, $x \in \langle 0, L\rangle$ [m], where L is the length of the vocal fold $L = 6.8$ [mm]. A constant vocal fold density ρ_h is assumed and the three dimensionality is addressed by assuming a uniform distribution of the aerodynamic quantities along the depth of the vocal fold h (dimension in the third direction). Further, the channel half-width (at time $t=0$) is chosen as $H_0 = \max_{x\in\langle 0,L\rangle} a(x) + g_0$, where g_0 is the initial half-gap, i.e. $g(0) = 2g_0$. The subglottal part of the length L_0 as well as the supraglottal part of the length L_2 was separated from the vocal folds part of the length L by the two very narrow and deep slots enabling to model the vertical motion of the vocal fold at the points of the channel discontinuity, i.e. between the parts Γ_{Wt} and Γ_D (see Fig. 4). This buffer zone does not influence the flow because the vibration amplitudes are very small up to the flutter instability and they are situated inside the boundary layer.

In the numerical simulations, the following slot dimensions were used: $\Delta L/L = 0.02$ and $\Delta H_0/L = 0.05 - 0.2$ depending on g_0 in order to avoid collisions of the masses m_1 and m_2 at the bottom of the slot.

2.2 Arbitrary Lagrangian Eulerian method

In order to treat the fluid flow on moving domains, the so-called Arbitrary Lagrangian Eulerian method is used, cf. [19]. We assume that $\mathcal{A} = \mathcal{A}(\xi,t) = \mathcal{A}_t(\xi)$ to be an ALE mapping defined for all $t \in (0,T)$ and $\xi \in \Omega_0$, which is smooth enough and continuously differentiable mapping of Ω_0 onto Ω_t. We define the *domain velocity* $\mathbf{w}_D = \mathbf{w}_D(x,t)$ defined

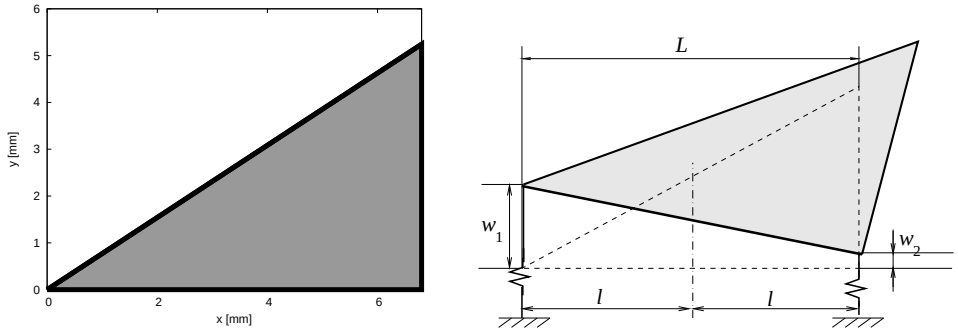

Figure 1: The considered geometry of the vocal folds for the female model F (left) and example of the vocal fold in displaced position (right).

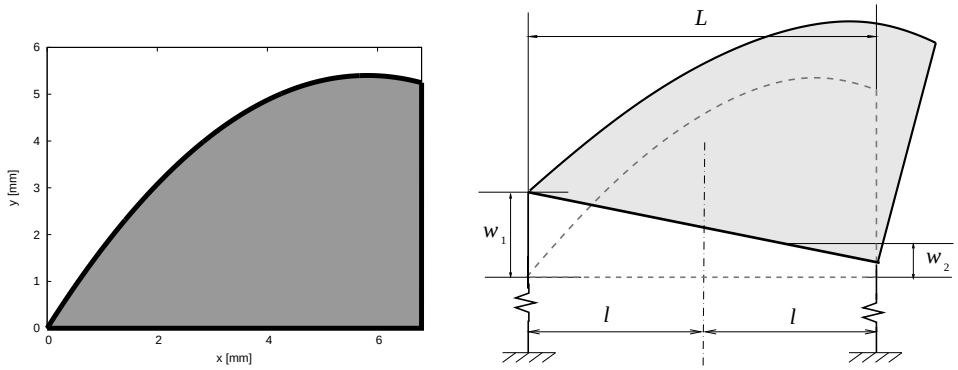

Figure 2: The considered geometry of the vocal folds for the male model M (left) and example of the vocal fold in displaced position (right).

for any $x\in\Omega_t$ and $t\in(0,T)$ by

$$\mathbf{w}_D(\mathcal{A}(\xi,t),t)=\frac{\partial\mathcal{A}}{\partial t}(\xi,t),\qquad \text{for all } \xi\in\Omega_0 \text{ and } t\in(0,T). \tag{2.1}$$

Furthermore the symbol $D^{\mathcal{A}}/Dt$ denotes the ALE derivative, i.e. the time derivative with respect to the reference configuration. For the ALE derivative holds

$$\frac{D^{\mathcal{A}}f}{Dt}(x,t)=\frac{\partial f}{\partial t}(x,t)+\mathbf{w}_D(x,t)\cdot\nabla f(x,t). \tag{2.2}$$

2.3 Flow model

The fluid flow is governed by the incompressible Navier-Stokes equations written in ALE form

$$\frac{D^{\mathcal{A}}\mathbf{v}}{Dt}+\big((\mathbf{v}-\mathbf{w}_D)\cdot\nabla\big)\mathbf{v}-\nu\triangle\mathbf{v}+\nabla p=0,\qquad \nabla\cdot\mathbf{v}=0,\qquad \text{in } \Omega_t, \tag{2.3}$$

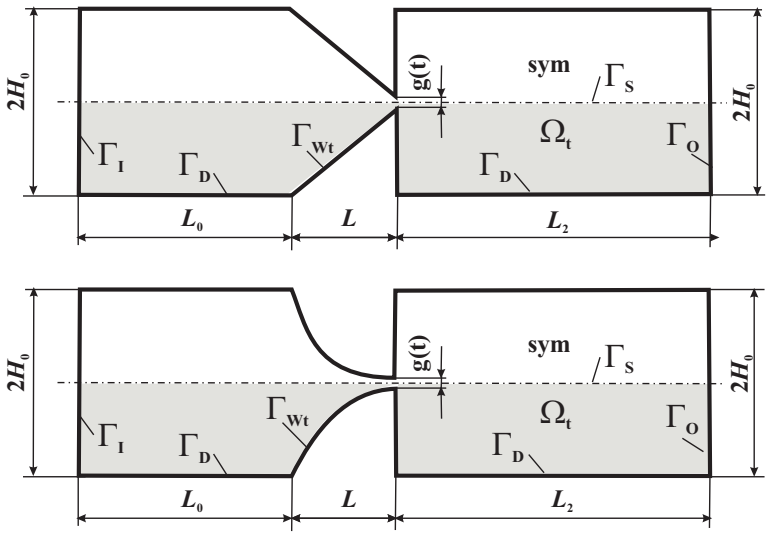

Figure 3: The computational domain Ω_t for models F (above) and M (bellow) surrounding the vocal fold shape given by $a_f(x)$ and $a_m(x)$, respectively. The lower shaded part is used for computations assuming the symmetry boundary condition on the axis of symmetry.

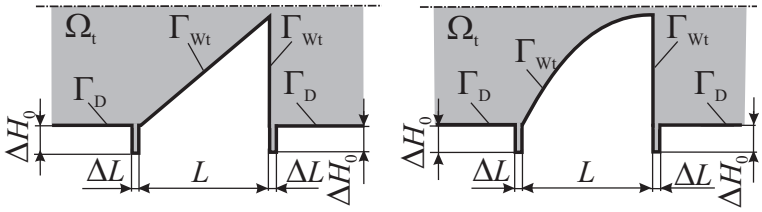

Figure 4: The detail of buffer zone.

where $\mathbf{v}=\mathbf{v}(x,t)$ is the flow velocity vector ($\mathbf{v}=(v_1,v_2)^T$), $p=p(x,t)$ is the kinematic pressure (i.e. pressure divided by the constant fluid density ρ), ν is the kinematic viscosity.

The boundary of the computational domain $\partial\Omega_t$ consists of mutually disjoint parts Γ_D (wall), Γ_I (inlet), Γ_O (outlet), Γ_S (axis of symmetry) and the moving part Γ_{Wt} (oscillating wall). The following boundary conditions are prescribed

$$\mathbf{v}(x,t)=\mathbf{0}, \quad \text{for } x\in\Gamma_D, \tag{2.4a}$$

$$\mathbf{v}(x,t)=\mathbf{w}_D(x,t), \quad \text{for } x\in\Gamma_{Wt}, \tag{2.4b}$$

$$v_2=0, \quad \frac{\partial v_1}{\partial y}=0, \quad \text{on } \Gamma_S, \tag{2.4c}$$

$$-(p-p_{ref})\mathbf{n}+\frac{1}{2}(\mathbf{v}\cdot\mathbf{n})^{-}\mathbf{v}+\nu\frac{\partial\mathbf{v}}{\partial\mathbf{n}}=0, \quad \text{on } \Gamma_O, \tag{2.4d}$$

where $\mathbf{n}$ denotes the unit outward normal vector, p_{ref} denotes a reference pressure value and α^- denotes the negative part of a real number α, see also [5, 11]. On the inlet one of the two following conditions is used on Γ_I

$$-(p-p_{inlet})\mathbf{n}+\frac{1}{2}(\mathbf{v}\cdot\mathbf{n})^-\mathbf{v}+\nu\frac{\partial\mathbf{v}}{\partial\mathbf{n}}=0, \tag{2.5a}$$

$$\text{or} \quad \mathbf{v}(x,t)=(V_0,0)^T, \tag{2.5b}$$

which means that either *the inlet flow velocity* V_0 is given – Eq. (2.5b) – or *the inlet pressure* is prescribed $p_{inlet}=p_{ref}+\Delta p$ – Eq. (2.5a). The reference pressure p_{ref} can be chosen arbitrarily, for what follows we set $p_{ref}=0$. Finally, we prescribe the initial condition $\mathbf{v}(x,0)=\mathbf{v}^0(x)$ for $x\in\Omega_0$. The initial configuration Ω_0 is shown in Fig. 3 for the channel shapes considered for the models F and M, respectively.

2.4 Structure model

The vibrating part (vocal folds) of the channel walls is governed by an aeroelastic two degrees of freedom model, i.e. the motion of Γ_{Wt} is driven by the displacements $w_1(t)$ and $w_2(t)$ (upward positive) of the two masses m_1 and m_2, respectively (see Fig. 5). The displacements $w_1(t)$ and $w_2(t)$ are then described by the following equations (see [14] for details)

$$\mathbb{M}\begin{pmatrix}\ddot{w}_1\\ \ddot{w}_2\end{pmatrix}+\mathbb{B}\begin{pmatrix}\dot{w}_1\\ \dot{w}_2\end{pmatrix}+\mathbb{K}\begin{pmatrix}w_1\\ w_2\end{pmatrix}=\begin{pmatrix}-F_1\\ -F_2\end{pmatrix}, \tag{2.6}$$

where $\mathbb{M}$ and $\mathbb{K}$ are the mass and stiffness matrices, respectively, given by

$$\mathbb{M}=\begin{pmatrix}m_1+\frac{m_3}{4} & \frac{m_3}{4}\\ \frac{m_3}{4} & m_2+\frac{m_3}{4}\end{pmatrix}, \qquad \mathbb{K}=\begin{pmatrix}c_1 & 0\\ 0 & c_2\end{pmatrix},$$

where m_1,m_2,m_3 are the equivalent masses, c_1,c_2 are the spring constants,

$$\mathbb{B}=\varepsilon_1\mathbb{M}+\varepsilon_2\mathbb{K}$$

is the matrix of the proportional structural damping where ε_1, ε_2 are the proportional damping coefficients (see [15, 16]) and F_1,F_2 are the aerodynamic forces (downward positive).

2.5 Coupling conditions

The fluid flow model (2.3) is coupled with the equation of motion (2.6) by interface conditions. First, the boundary condition (2.4b) must be satisfied on Γ_{Wt} where the domain velocity is given by Eq. (2.1). Further, the aerodynamic forces F_1,F_2 in (2.6) depend on flow velocity $\mathbf{v}$ and pressure p. The forces F_1 and F_2 are computed with the aid of the aerodynamical lift force F_L and the aerodynamical torsional moment M as

$$F_1(t)=-\frac{F_L(t)}{2}-\frac{1}{2l}M(t), \qquad F_2(t)=-\frac{F_L(t)}{2}+\frac{1}{2l}M(t), \tag{2.7}$$

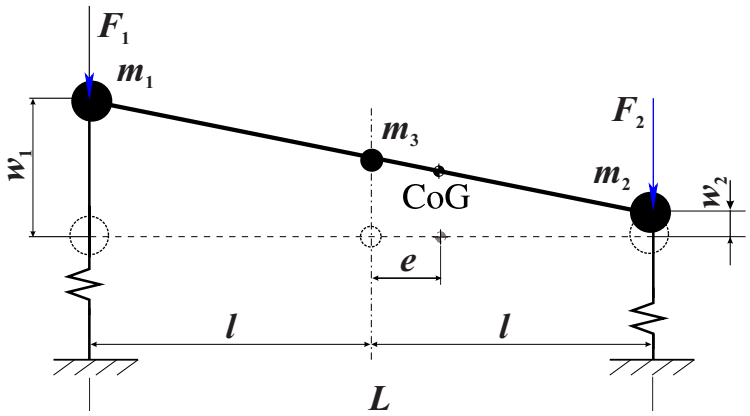

Figure 5: Aeroelastic two degrees of freedom model (with masses m_1, m_2, m_3) in displaced position (displacements w_1 and w_2) and resulting aerodynamic forces F_1 and F_2.

where l denotes the distance of the masses m_1 and m_2 from the center (see Fig. 5). The aerodynamical quantities are evaluated as follows

$$F_L(t) = h\int_{\Gamma_{Wt}} \sum_{j=1}^{2} \tau_{2j} n_j dS, \qquad M(t) = -h\int_{\Gamma_{Wt}} \sum_{i,j=1}^{2} \tau_{ij} n_j r_i^{\text{ort}} dS, \tag{2.8}$$

where $r_1^{\text{ort}} = -(x_2 - x_{C2})$, $r_2^{\text{ort}} = x_1 - x_{C1}$ and

$$\tau_{ij} = \rho\left[-p\delta_{ij} + \nu\left(\frac{\partial v_i}{\partial x_j} + \frac{\partial v_j}{\partial x_i}\right)\right].$$

By τ_{ij} we denote the components of the stress tensor, δ_{ij} denotes the Kronecker symbol, $\mathbf{n} = (n_1, n_2)$ is the unit outer normal to $\partial\Omega_t$ on Γ_{Wt} and $(x_{C1}, x_{C2}) = (0, L/2)$.

Furthermore, the transformation of the vocal fold surface at time instant t with the given reference $(\xi_1, \xi_2) \in \Gamma_{W0}$ is given by $\mathcal{A}_t(\xi_1, \xi_2) = (X, \xi_2)$ where

$$X = \xi_1 + \frac{1}{2l}\left[(L/2 + l - \xi_1) w_1(t) + (\xi_1 - L/2 + l) w_2(t)\right], \tag{2.9}$$

and where the displacements in x-direction were neglected (possible for small values of w_1, w_2). The ALE mapping is then at every time instant t obtained by an extension from Γ_{W0} on Ω_0, cf. [21, 23].

3 Numerical approximation

In this section the numerical approximation of the mathematical model presented in Section 2 is briefly described, a more detailed description can be found e.g. in [21].

3.1 Time discretization

We consider a partition $0=t_0<t_1<\cdots<T$, $t_k=k\Delta t$, with a constant time step $\Delta t>0$, of the time interval $(0,T)$ and approximate the solution $\mathbf{v}(\cdot,t_n)$ and $p(\cdot,t_n)$ (defined in Ω_{t_n}) at time t_n by $\mathbf{v}^n$ and p^n, respectively. For the time discretization the second order backward difference formula (BDF2) is applied, i.e.

$$\frac{D^{\mathcal{A}}\mathbf{v}}{Dt}(x,t^{n+1})\approx\frac{3\mathbf{v}^{n+1}-4\hat{\mathbf{v}}^n+\hat{\mathbf{v}}^{n-1}}{2\Delta t},\qquad \text{where } x\in\Omega_{n+1}, \tag{3.1}$$

where $\hat{\mathbf{v}}^n$ and $\hat{\mathbf{v}}^{n-1}$ are the approximate solutions $\mathbf{v}^n$ and $\mathbf{v}^{n-1}$ defined on Ω_n and Ω_{n-1}, respectively, and transformed onto Ω_{n+1}. Further, we approximate the domain velocity $\mathbf{w}_D(x,t_{n+1})$ by $\mathbf{w}_D^{n+1}$, where

$$\mathbf{w}_D^{n+1}(x)=\frac{3\mathcal{A}_{t_{n+1}}(\xi)-4\mathcal{A}_{t_n}(\xi)+\mathcal{A}_{t_{n-1}}(\xi)}{2\Delta t},\qquad x=\mathcal{A}_{t_{n+1}}(\xi),\quad x\in\Omega_{n+1}.$$

Then the time discretization leads to the following problem in domain Ω_{n+1}

$$\frac{3\mathbf{v}^{n+1}-4\hat{\mathbf{v}}^n+\hat{\mathbf{v}}^{n-1}}{2\Delta t}-\nu\triangle\mathbf{v}^{n+1}+\Big((\mathbf{v}^{n+1}-\mathbf{w}_D^{n+1})\cdot\nabla\Big)\mathbf{v}^{n+1}+\nabla p^{n+1}=0, \tag{3.2a}$$

$$\nabla\cdot\mathbf{v}^{n+1}=0, \tag{3.2b}$$

equipped with boundary conditions (2.4) and (2.5a). Here, we do not consider the weak formulation of the inlet velocity condition (2.5b), that is more simple to treat compared to the inlet pressure condition (2.5a).

3.2 Weak formulation and spatial discretization

For solving of Eq. (2.3) by FE method, the time-discretized problem is reformulated in a weak sense. By $\mathbf{W}=\mathbf{H}^1(\Omega_{n+1})$ the velocity space is defined, by $\mathbf{X}\subset\mathbf{W}$ the sub-space of test functions being zero on the Dirichlet part of the boundary is denoted as

$$\mathbf{X}=\big\{\boldsymbol{\varphi}=(\varphi_1,\varphi_2)\in W\colon \boldsymbol{\varphi}=0 \text{ on } \Gamma_{Wt_{n+1}}\cap\Gamma_D,\ \varphi_2=0 \text{ on } \Gamma_S\big\},$$

and by $Q=L^2(\Omega_{n+1})$ the pressure space is denoted. Using the standard approach, cf. [21], the solution $\mathbf{v}=\mathbf{v}^{n+1}$ and $p=p^{n+1}$ of problem (2.3) satisfies

$$a(U,V)+\mathcal{B}(U,V)=f(V),\qquad U=(\mathbf{v},p) \tag{3.3}$$

for all $V=(\mathbf{z},q)\in\mathbf{X}\times Q$, where

$$a(U,V)=\left(\frac{3}{2\Delta t}\mathbf{v},\mathbf{z}\right)+\nu(\nabla\mathbf{v},\nabla\mathbf{z})+c_n(\mathbf{v};\mathbf{v},\mathbf{z})-(p,\nabla\cdot\mathbf{z})+(\nabla\cdot\mathbf{v},q), \tag{3.4a}$$

$$c_n(\mathbf{w},\mathbf{v},\mathbf{z})=\int\limits_{\Omega_{n+1}}\left(\frac{1}{2}(\mathbf{w}\cdot\nabla\mathbf{v})\cdot\mathbf{z}-\frac{1}{2}(\mathbf{w}\cdot\nabla\mathbf{z})\cdot\mathbf{v}-(\mathbf{w}_D^{n+1}\cdot\nabla)\mathbf{v}\cdot\mathbf{z}\right)dx, \tag{3.4b}$$

$$\mathcal{B}(U,V)=\int\limits_{\Gamma_I\cup\Gamma_O}\frac{1}{2}(\mathbf{v}\cdot\mathbf{n})^+\mathbf{v}\cdot\mathbf{z}dS, \tag{3.4c}$$

$$f(V)=\frac{1}{2\Delta t}\left(4\hat{\mathbf{v}}^n-\hat{\mathbf{v}}^{n-1},\mathbf{z}\right)-\int_{\Gamma_I}p_{inlet}\mathbf{v}\cdot\mathbf{n}dS-\int_{\Gamma_O}p_{ref}\mathbf{v}\cdot\mathbf{n}dS, \tag{3.4d}$$

$U=(\mathbf{v},p)$, $V=(\mathbf{z},q)$ and by $(\cdot,\cdot)$ we denote the scalar product in the space $L^2(\Omega_{n+1})$.

Further, the weak formulation is approximated by the use of FEM: we restrict the couple of spaces (X,M) to FE spaces (X_h,M_h) and the computational domain Ω_t is approximated by an admissible triangulation $\mathcal{T}_h$. Based on the triangulation $\mathcal{T}_h$ the equal order finite elements are used, and the Galerkin Least-Squares(GLS) stabilized method is applied, [10].

3.3 Coupling algorithm

The motion equations are discretized in time with the aid of the 2nd or 4th order backward difference formula and the coupled fluid-structure model is solved with the aid of partitioned strongly coupled scheme, which enforces both the dynamical coupling conditions (2.7), (2.8) and the kinematical condition (2.4b). In the practical implementation the fluid flow and the structure motion are approximated repeatedly per every time step in order to converge to a solution which satisfy both conditions. The detailed description of the numerical approximation of a similar coupled model can be found, e.g. in [21].

4 Numerical results

For the numerical analysis the following parameters were used. The three masses m_1,m_2,m_3 were determined by

$$m_{1,2}=\frac{1}{2l^2}(I+me^2\pm mel),\qquad m=m_1+m_2+m_3, \tag{4.1}$$

where the distance of the masses m_1 and m_2 from the center was $l=L/2$ (see Fig. 5), and the total mass m of the vocal folds, the inertia moment I and the eccentricity e were computed using the vocal fold shape and its density $\rho_h=1020$ kg/m^3, length (depth of the channel) $h=18$ mm and thickness $L=6.8$ mm, see [16] for details. The fluid density was $\rho=1.2$ kg/m^3 and the kinematic viscosity $\nu=1.58\times10^{-5}$m^2/s. In all the computations the following sub-glottal and supra-glottal lengths were used $L_0=4\times L$, $L_2=4\times L$ (see Fig. 3).

4.1 Aeroelastic simulations for model F with inlet pressure condition

First, the problem of interaction of air flow with aeroelastic model F shown in Fig. 1 was considered with the inlet pressure boundary condition. The considered initial half-gap was chosen $g_0 = 0.3$ mm. The structural parameters and the natural frequencies f_1, f_2 for the structure vibrating in vacuo are listed in Table 1. The computations were performed in the computational domain Ω_t shown in Fig. 3, where $H_0 = 5.54416$ mm. The displacement of the vocal fold part denoted by Γ_{Wt} with the length L was given by (2.9).

Table 1: Structural parameters considered for the *model F*.

Input data for model F			
shape	$a_f(x)$	f_1 [Hz]	100
m [kg]	3.274×10^{-4}	f_2 [Hz]	160
I [kg/m^2]	1.341×10^{-9}	c_1 [N/m]	44.8
e [m]	1.133×10^{-3}	c_2 [N/m]	84.6
ε_1[s^{-1}]	120.35	ε_2 [s]	6.12×10^{-5}

On the inlet the pressure was prescribed and the problem was approximated using the inlet pressure formulation. The results are shown in Fig. 6, where the aeroelastic response $w_1(t)$, $w_2(t)$ and the mean inlet velocity in dependence on time t are shown for several prescribed pressure differences $\Delta p \approx 100-3200$ Pa (inlet velocity V_0 oscillated around $V_0 \approx 0.55-3.13$ m/s). In this range, the simplified method in [15] predicted the aeroelastic instability of type flutter for the inlet velocity $V_{crit} = 0.87$ m/s, but in the mentioned paper the inlet/outlet velocity formulation was used.

The vibrations of the vocal fold in Fig. 6 dies out for all the values of the inlet pressure with no significant decrease or increase of the aerodynamic damping. Particularly, the (aerodynamic) damping is quite strong for all the studied cases. The aeroelastic instability was never observed for the physically relevant values of the inlet pressure (values of Δp up to 5000 Pa were tested). This behaviour is probably caused by "additional damping" effects due to the inlet pressure boundary condition prescribed. Particularly, in Fig. 6 the inlet velocity oscillations are shown, where the inlet velocity is increasing with a wider opening of the glottal part $g(t)$ and similarly decreasing with a narrower enclosure of $g(t)$. The inlet velocity oscillations (as well as consequently the flow rate oscillations) influence the aerodynamic forces and are leading to damped vibrations of the structure.

4.2 Aeroelastic simulations for model F with inlet velocity condition

The problem with the same input parameters used in Section 4.1 was also numerically analyzed with the inlet velocity boundary condition.

The values of the inlet velocity V_0 were considered in the range $0.2-0.7$ m/s in order to detect the critical velocity for the flutter type of aeroelastic instability leading to self-sustained vibrations of the vocal fold. The aeroelastic responses are shown in Fig. 7 for

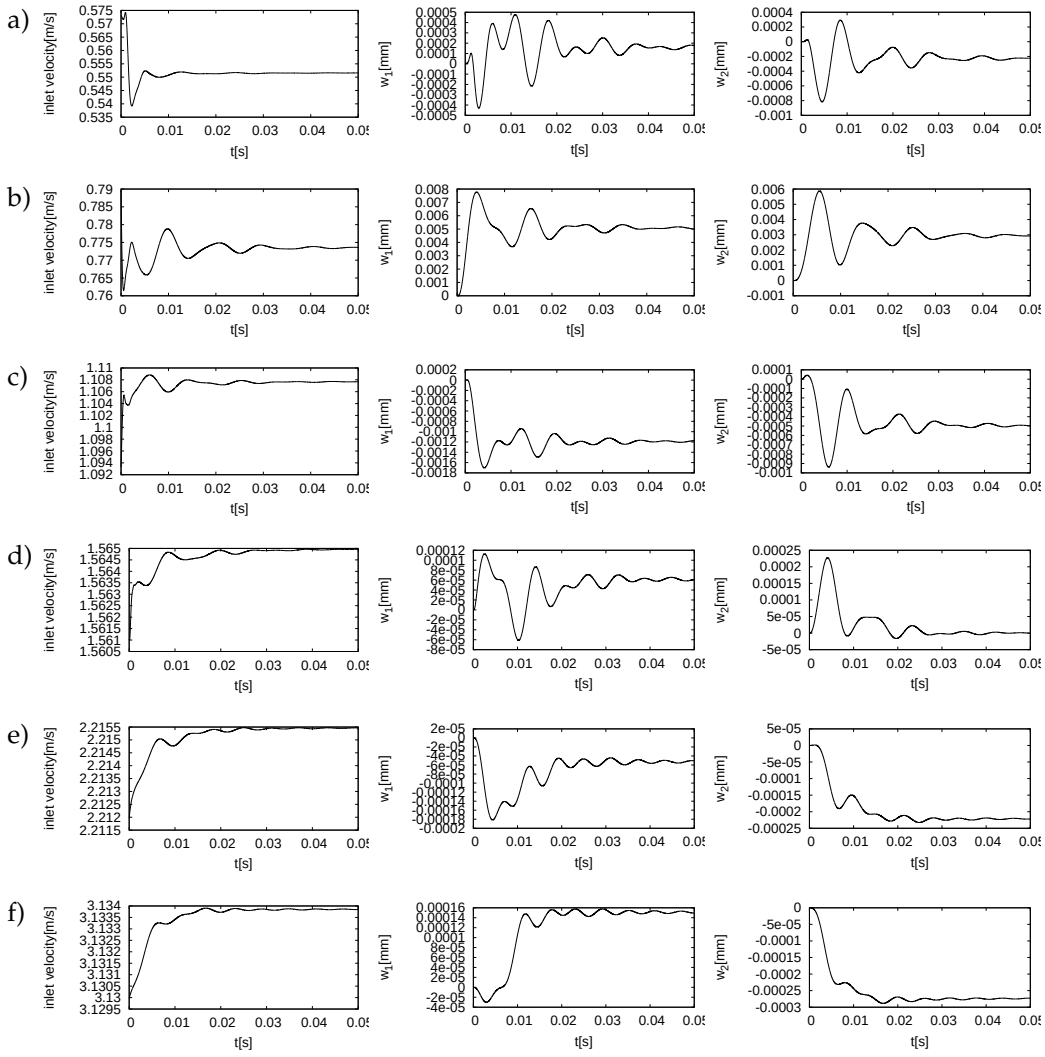

Figure 6: The mean inlet velocity oscillations (left column) and the aeroelastic response of the system $w_1(t)$, $w_2(t)$ (middle and right columns) for *model F* and the prescribed inlet pressure boundary conditions. The inlet pressure was chosen a) $\Delta p = 100$ Pa, b) $\Delta p = 200$ Pa, c) $\Delta p = 400$ Pa, d) $\Delta p = 800$ Pa, e) $\Delta p = 1600$ Pa, f) $\Delta p = 3200$ Pa.

the inlet velocities $V_0 = 0.45$ m/s, $V_0 = 0.55$ m/s, $V_0 = 0.6$ m/s and $V_0 = 0.65$ m/s. For the velocities 0.45 m/s and 0.55 m/s the structural vibrations are damped in time and the aeroelastic system is stable. Nevertheless, the aerodynamical damping for the velocity 0.55 m/s is weaker compared to the lower inlet velocity result. With the further increase of the inlet velocity to $V_0 = 0.6$ m/s the self oscillations can be observed in Fig. 7c). For the inlet velocity $V_0 = 0.65$ m/s the vibrations of the vocal folds are growing very fast (see Fig. 7d). The simulation for $V_0 = 0.65$ m/s is only shown in the time interval to 0.175 s, where the computations crashed due to the high distortion of the computational mesh.

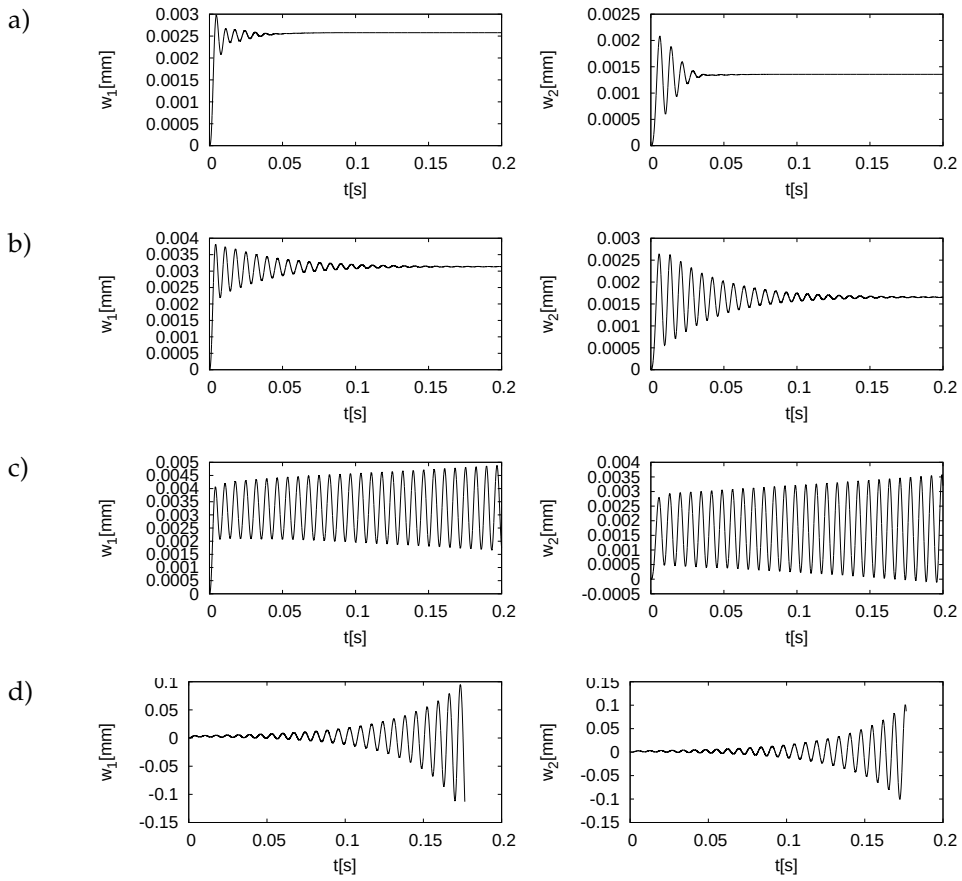

Figure 7: The aeroelastic response of the aeroelastic system for *model F* with the prescribed inlet velocity; the graphs of $w_1(t)$, $w_2(t)$ in dependence on time t are shown for the different inlet velocities a) $V_0 = 0.45m/s$, b) $V_0 = 0.55m/s$, c) $V_0 = 0.6m/s$ and d) $V_0 = 0.65m/s$.

4.3 Aeroelastic simulations for model M

Furthermore, the aeroelastic model of flow interaction with the vocal fold given by the parabolic shape $a_m(x)$ shown in Fig. 2 was analyzed. For this case the considered initial half-gap was $g_0 = 0.3\,\text{mm}$, $H_0 = 5.7\,\text{mm}$ and the structural parameters are listed in Table 2 (see also [15, 16]). The aeroelastic response $w_1(t)$, $w_2(t)$ is shown in Fig. 8 and plotted over time in terms of displacements for inlet flow velocities $V_0 = 1.0 - 1.2\,\text{m/s}$. For the inlet velocities lower or equal to 1.1 m/s the vocal fold oscillations die in time due to both structural and aerodynamic damping. For the flow velocity $V_0 = 1.15\,\text{m/s}$ the self-oscillations of the vocal folds were obtained.

Simulation examples of the flow velocity distribution in the glottis during the aeroelastic instability for $V_0 = 1.5\,\text{m/s}$ are shown in Fig. 9 at several time instants marked in the graph of $w_1(t)$ and $w_2(t)$. The maximal flow velocities in the channel are increasing when the glottal gap is becoming narrower, i.e. for high values of $w_2(t)$; the maximum

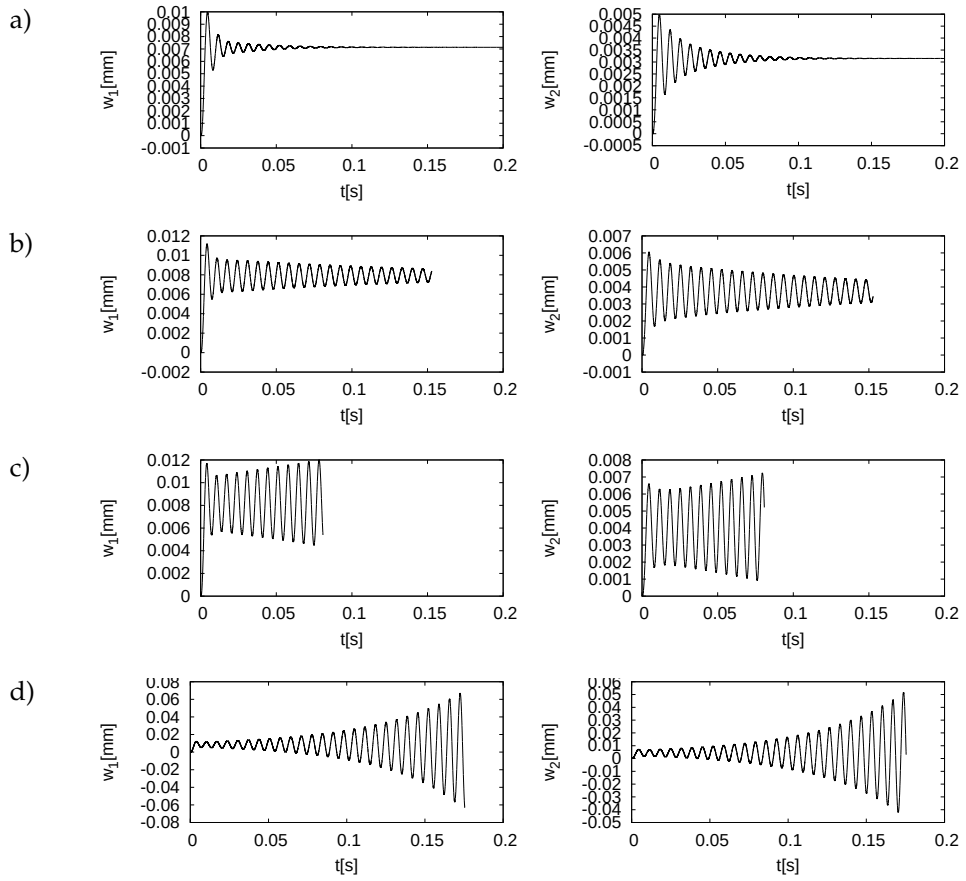

Figure 8: The response of the aeroelastic system for *model M* with the prescribed inlet velocity boundary condition; the graphs of $w_1(t)$, $w_2(t)$ in dependence on time t are shown for the different inlet velocities a) $V_0=1.0m/s$, b) $V_0=1.1m/s$, c) $V_0=1.15m/s$ and d) $V_0=1.2m/s$.

Table 2: Structural parameters considered for the *model M*.

Input data for model M			
shape	$a_m(x)$	f_1 [Hz]	100
m [kg]	4.812×10^{-4}	f_2 [Hz]	160
I [kg/m^2]	2.351×10^{-9}	c_1 [N/m]	56
e [m]	0.771×10^{-3}	c_2 [N/m]	174.3
ε_1[s^{-1}]	120.35	$\varepsilon_2[s]$	6.12×10^{-5}

flow velocity in the glottal gap is lower than 40 m/s, which is in agreement with reality. Small changes in the position of the flow separation point on the vocal fold surface can be also detected in the flow field patterns in the glottal gap (see e.g. the details in Fig. 9 at the time t_3 and t_5).

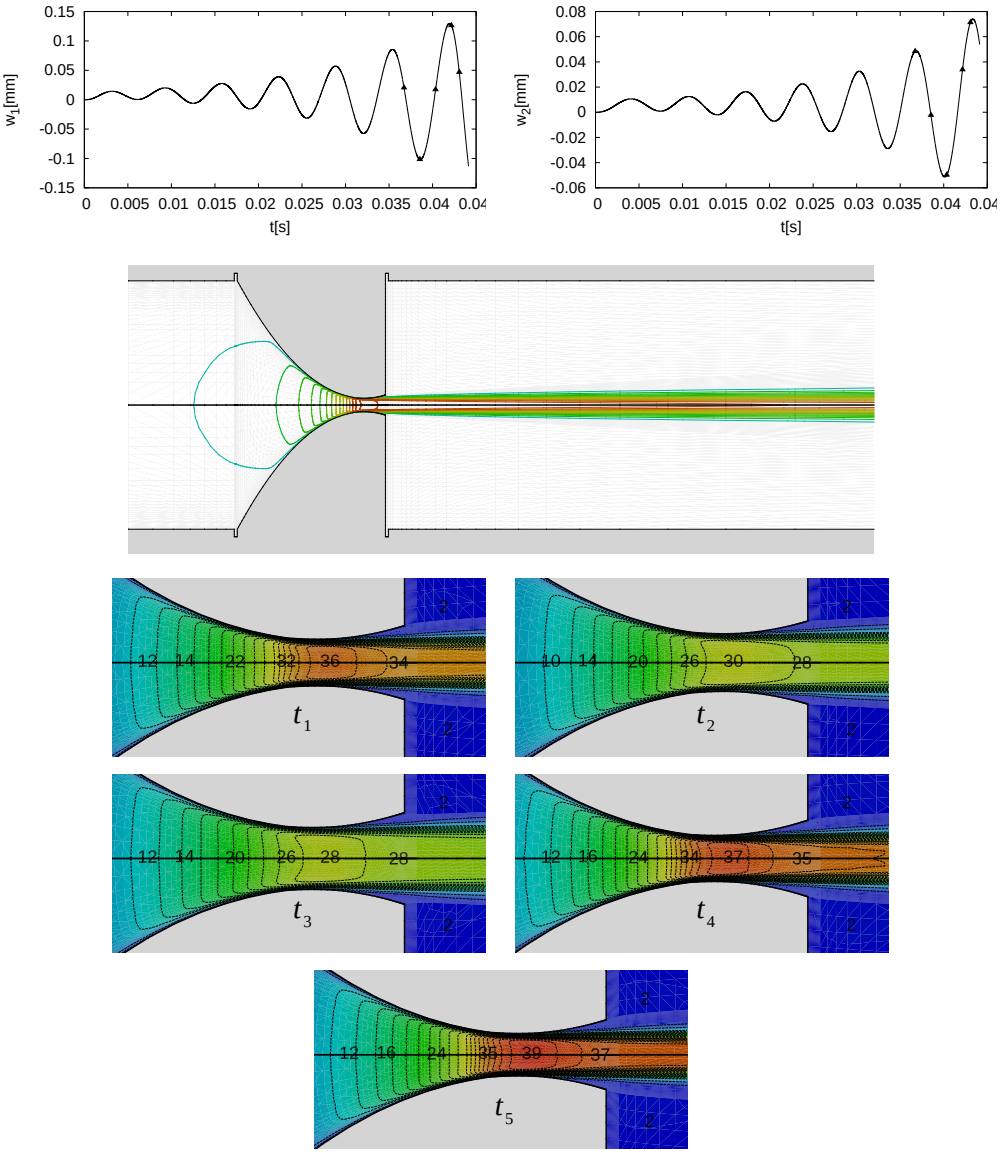

Figure 9: The aeroelastic response $w_1(t)$, $w_2(t)$ for *model M* for the inlet velocity 1.5 m/s (above). The flow velocity isolines in the channel (middle panel) with details in the glottal gap (bellow) shown at five time instants t_1, t_2, $\cdots$, t_5 marked in the graphs of $w_1(t)$ and $w_2(t)$.

4.4 Comparison of the results with simplified theory

The results obtained by the developed numerical method based on the FE solution of the 2D Navier-Stokes equations are compared with the results computed by the perturbation theory for 1D potential flow model [15] in Fig. 10. The computed flutter airflow velocities $V_{0,flutter}$, the pressure drop $\Delta p_{flutter}$, i.e. the so-called phonation threshold pressures

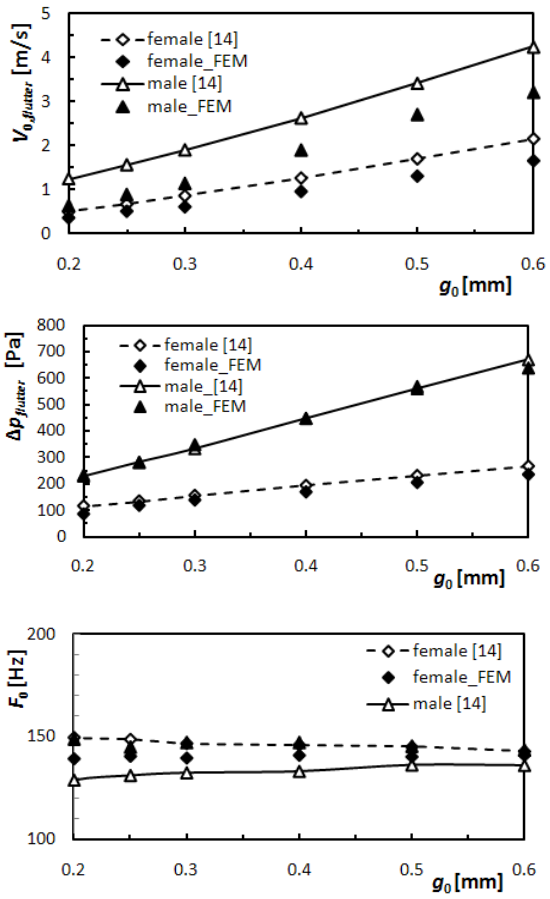

Figure 10: Comparison of the flutter velocities, the sub-glottal pressures (phonation threshold pressures – PTP) and the flutter (phonation) frequencies computed by the FE method with the simplified flow theory [14–16].

(PTP), and the flutter frequencies F_0, i.e. the so-called fundamental phonation frequencies, are shown in dependence on the prephonatory glottal half gap g_0 for the male and female models of the vocal folds. The computed results: $V_{0,flutter} \approx 0.5-4$ m/s (corresponding to the flow rates $0.1-0.9$ l/s), $\Delta p_{flutter} \approx 100-700$ Pa and $F_0 \approx 130-150$ Hz are in physiologically relevant intervals for the phonation threshold in humans; the values for $V_{0,flutter}$ and $\Delta p_{flutter}$ for the female model are lower than for the male model and the opposite is valid for the phonation frequencies; the computed values $V_{0,flutter}$ and $\Delta p_{flutter}$ increase with the prephonatory glottal half-gap g_0 (see e.g. [2, 13, 14]).

In general, the flutter velocities $V_{0,flutter}$ resulting from the FE simulations are lower than the flutter velocities computed according to the simplified theory presented in [15]. These differences (see Fig. 10) can be explained by the fluid viscosity considered in the FE simulations because the developed boundary layer on the surface of the vocal fold model results in narrowing of the glottal gap g_0. The second reason can be the position

of the flow separation point which was in [15] artificially fixed at the vocal fold supraglottal edge, however, according to the FE computations the flow separation point was slightly moving (see Fig. 9). These differences are smaller for the female model because the triangle shape satisfies better the conditions used in the simplified theory. The difference between the FE results and the results of the simplified theory [15] for the critical pressure drops $\Delta p_{flutter}$ and the flutter frequencies F_0 is much smaller (see Fig. 10).

5 Conclusion

In this paper the coupled FSI problem of air flow through a vibrating glottal region was numerically analyzed using finite element solution of the Navier-Stokes equations and the comparison to the results obtained by the simplified flow theory [15, 16] was presented. An attention was paid to investigation of the flutter boundary for which self-sustained vibrations of vocal folds occur: the physical meaning of such instability is the so-called phonation onset which is an important voice production characteristic in humans.

The aeroelastic response was studied in dependence on the type of the inlet boundary condition used. The inlet pressure and inlet velocity formulations were used, and the numerical results for the case with the same geometrical shape and the same structural parameters were compared. For the inlet pressure boundary condition the vibrations of the vocal fold were strongly damped for all values of the inlet pressure in the range corresponding to physiological flow rates and no self oscillations were observed. In the same range of the flow rates with the prescribed inlet velocity the self-sustained oscillations were obtained. The results show that the presence of self oscillations of vocal folds is influenced by the prescribed inlet boundary condition. This is extremely important as the in- and out-let boundary conditions are the "artificial boundaries" for which the values of aerodynamical quantities are only known approximately.

Furthermore, the numerical results of the simulations for two different aeroelastic problems were compared to the results computed by the simplified theory published in [15, 16], yielding acceptable agreement in the prediction of the aeroelastic instability, especially the so-called phonation threshold pressure given by the flutter type of instability. The agreement in the critical pressure drop is good, although there is a difference in the predicted flutter velocity. This can be caused by several necessary simplifications used in [15] and [16], where the fluid viscosity was neglected and the flow separation was assumed strictly at the outflow edge of the vocal folds (see also [8] for similar analysis).

The developed numerical method for finding the phonation onset parameters given by the aeroelastic instability of the vocal folds is much more complex than the mathematical model studied in the papers [14–16], and for the channel flow gives more accurate and detailed information on the flow field pattern in the glottis. Nevertheless, one needs to face several difficulties, which are not treated in the original mathematical model. Particularly, as for the approximate solution of the Navier-Stokes equations the use of highly

distorted meshes is not possible and the motion of the vocal folds must be smoothed by a neighbouring buffer zone not considered in the mentioned papers.

Acknowledgments

This research was supported by the Project OC 09019 "Modelling of voice production based on biomechanics" within the program COST of the Ministry of Education of the Czech Republic, under grants No. 201/08/0012 and No. P101/11/0207 of the Grant Agency of the Czech Republic and the Research Plan MSM 6840770003 of the Ministry of Education of the Czech Republic.

References

[1] P. Alku, J. Horáček, M. Airas, F. Griffond-Boitier, and A. M. Laukkanen. Performance of glottal inverse filtering as tested by aeroelastic modelling of phonation and FE modelling of vocal tract. Acta Acustica united with Acustica, 92(5):717–724, 2006.

[2] R. J. Baken and R. F. Orlikoff. Clinical Measurement of Speech and Voice. Singular Publishing Group Inc., San Diego, California, 2nd edition, 2000.

[3] K. J. Bathe, editor. Computational Fluid and Solid Mechanics 2007. Elsevier, 2007.

[4] D. A. Berry, H. Herzel, R. Titze, and K. Krischer. Interpretation of biomechanical simulations of normal and chaotic vocal fold oscillations with empirical eigenfunctions. Journal of the Acoustical Society of America, 95(6):3595–3604, 1994.

[5] Ch.-H. Bruneau and P. Fabrie. Effective downstream boundary conditions for incompressible navierstokes equations. International Journal for Numerical Methods in Fluids, 19(8):693–705, 1994.

[6] R. Codina. Stabilization of incompressibility and convection through orthogonal sub-scales in finite element methods. Computational Method in Applied Mechanical Engineering, 190:1579–1599, 2000.

[7] T. A. Davis and I. S. Duff. A combined unifrontal/multifrontal method for unsymmetric sparse matrices. ACM Transactions on Mathematical Software, 25:1–19, 1999.

[8] M. P. de Vries, H. K. Shutte, A. E. P. Veldman, and G.J. Verkerke. Glottal flow through a two-mass model: Comparison of Navier-Stokes solutions with simplified models. Journal of Acoust. Soc. Am., 111(4):1847–1853, 2002.

[9] E. H. Dowell. A Modern Course in Aeroelasticity. Kluwer Academic Publishers, Dodrecht, 1995.

[10] T. Gelhard, G. Lube, M. A. Olshanskii, and J.-H. Starcke. Stabilized finite element schemes with LBB-stable elements for incompressible flows. Journal of Computational and Applied Mathematics, 177:243–267, 2005.

[11] J. G. Heywood, R. Rannacher, and S. Turek. Artificial boundaries and flux and pressure conditions for the incompressible Navier-Stokes equations. Int. J. Numer. Math. Fluids, 22:325–352, 1992.

[12] J. Horáček, A. M. Laukkanen, P. Šidlof, P. Murphy, and J. G. Švec. Comparison of acceleration and impact stress as possible loading factors in phonation. A computer modeling study. Folia Phoniatrica et Logopaedica, 61(3):137–145, 2009.

[13] J. Horáček, A.M. Laukkanen, and P. Šidlof. Estimation of impact stress using an aeroelastic model of voice production. Logopedics Phoniatrics Vocology, 37:185–192, 2007.
[14] J. Horáček, P. Šidlof, and J. G. Švec. Numerical simulation of self-oscillations of human vocal folds with Hertz model of impact forces. Journal of Fluids and Structures, 20(6):853–869, 2005.
[15] J. Horáček and J. G. Švec. Instability boundaries of a vocal fold modelled as a flexibly rigid body vibrating in a channel conveying fluid. AMD, American Society of Mechanical Engineers, Applied Mechanics Division, 253(2):1043–1054, 2002.
[16] J. Horáček and J. G. Švec. Aeroelastic model of vocal-fold-shaped vibrating element for studying the phonation threshold. Journal of Fluids and Structures, 16(7):931 – 955, 2002.
[17] K. Ishizaka and J. L. Flanagan. Synthesis of voiced sounds from a two-mass model of the vocal coords. The Bell System Technical Journal, 51:1233–1268, 1972.
[18] G. Link, M. Kaltenbacher, M. Breuer, and M. Döllinger. A 2D finite element scheme for fluid-solid-acoustic interactions and its application to human phonation. Computation Methods in Applied Mechanical Engineering, 198:3321–3334, 2009.
[19] T. Nomura and T. J. R. Hughes. An arbitrary Lagrangian-Eulerian finite element method for interaction of fluid and a rigid body. Computer Methods in Applied Mechanics and Engineering, 95:115–138, 1992.
[20] P. Punčochářová, J. Fürst, K. Kozel, and J. Horáček. Numerical simulation of compressible flow with low Mach number through oscillating glottis. In I. Zolotarev and J. Horáček, editors, Flow Induced Vibrations, Prague, 2008. Institute of Thermomechanics, AS CR.
[21] P. Sváček, M. Feistauer, and J. Horáček. Numerical simulation of flow induced airfoil vibrations with large amplitudes. Journal of Fluids and Structure, 23(3):391–411, 2007.
[22] I. R. Titze. Physiologic and acoustic differences between male and female voices. Journal of the Acoustical Society of America, 85(4):1699–1707, 1989.
[23] Z. Yang and D. J. Mavriplis. Unstructured dynamic meshes with higher-order time integration schemes for the unsteady Navier-Stokes equations. In 43rd AIAA Aerospace Sciences Meeting, page 13 pp., Reno NV, January 2005. AIAA Paper 2005-1222.